Sequential decay analysis of ^{235}U($n^{\rm th}$, f) reaction using fragmentation approach

Nitin Sharma† Ashutosh Kaushik Manoj K. Sharma

School of Physics and Materials Science, Thapar Institute of Engineering & Technology, Patiala - 147004, Punjab, India

Abstract: Numerous experimental and theoretical observations have concluded that the probability of the three fragment emission (ternary fission) or binary fission increases when one proceeds towards the heavy mass region of nuclear periodic table. Many factors affect fragment emission, such as the shell effect, deformation, orientation, and fissility parameter. Binary and ternary fissions are observed for both ground and excited states of the nuclei. The collinear cluster tripartition (CCT) channel of the ^{235}U($n^{\rm th}$, f) reaction is studied, and we observe that the CCT may be a sequential or simultaneous emission phenomenon. To date, different approaches have been introduced to study the CCT process as a simultaneous or sequential process, but the decay dynamics of these modes have not been not fully explored. Identifying the three fragments of the sequential process and exploring their related dynamics using an excitation energy dependent approach would be of further interest. Hence, in this study, we investigate the sequential decay mechanism of the ^{235}U($n^{\rm th}$, f) reaction using quantum mechanical fragmentation theory (QMFT). The decay mechanism is considered in two steps, where initially, the nucleus splits into an asymmetric channel. In the second step, the heavy fragment obtained in the first step divides into two fragments. Stage I analysis is conducted by calculating the fragmentation potential and preformation probability for the spherical and deformed choices of the decaying fragments. The most probable fragment combination of stage I are identified with respect to the dips in the fragmentation structure and the corresponding maxima of the preformation probability (P_0). The light fragments of the identified decay channels (obtained in step I) agree closely with the experimentally observed fragments. The excitation energy of the decay channel is calculated using an iteration process. The excitation energy is shared using an excitation energy dependent level density parameter. The obtained excitation energy of the identified heavy fragments is further used to analyze the fragmentation, and the subsequent binary fragments of the sequential process are obtained. The three identified fragments of the sequential process agree with experimental observations and are found near the neutron or proton shell closure. Finally, the kinetic energy of the observed fragments is calculated, and the middle fragment of the CCT mechanism is identified.

Keywords: fission, cluster radioactivity, ternary fission, spontaneous fission, cluster model, total kinetic energy, preformation probability

DOI: 10.1088/1674-1137/ad2dc1

I. INTRODUCTION

The irradiation of neutrons onto uranium isotopes revealed an important phenomenon known as nuclear fission [1]. It is a very complex phenomenon and still not fully understood as various tools and mechanisms are employed to understand the evolving process. The partitioning of a nucleus depends on various factors such as excitation energy, mass asymmetry, shell effect, and deformation. The decay dynamics of the nucleus also alters when transitioning from the lighter to heavy mass region. A major property of nuclei belonging to the heavy mass region is that they can decay into two or three fragments, and the process is termed binary or ternary fission, respectively. Binary emission of the decaying fragments is very common and fully understood, but ternary fission is a rare and a relatively complex process. Numerous experimental and theoretical attempts [2−11] have been made to understand the exotic ternary decay mechanism. Ref. [12] concluded that the main reason for the three fragment emission is the proton or neutron shell closure effect associated with the decaying fragments. The ternary

Received 19 December 2023; Accepted 27 February 2024; Published online 28 February 2024

† E-mail: nitinsharma2295@gmail.com

decay mechanism is basically of two types, *i.e.*, light particle accompanied fission (LCP) or true ternary fission (TTF), and both phenomena depend on the mass of the third fragment. In the LCP mode, a light third fragment is emitted, whereas in TTF, three fragments of comparable size are emitted. Ternary fission has two probable geometrical configurations: equatorial cluster tripartition (ECT) and collinear cluster tripartition (CCT). Studies [11, 13] have shown that the ECT process is suitable for the emission of the light third fragment, whereas the CCT process is suitable for both the light and heavy third fragment emission. Additionally, nuclear shapes play an important role in three fragment emission [14, 15].

The behaviour of the nuclei belonging to the heavy mass region was studied using the saddle point model [14, 16], and the studies suggested that two or three neck shapes are more probable when transitioning from the lighter to heavier mass region. Over the last few decades, different tools have been employed to explore the competitive behaviour of fissioning nuclei. Particular attention has been given to the thermal neutron induced fission of heavy nuclei. The mass distribution and related kinetics of three particle emission from the ^{235}U($n^{\rm th}$, f) reaction was studied experimentally by Schmitt *et al*. [17], who concluded that shell effects have an important role in both binary and ternary emission. Additionally, the neutron induced fission of ^{233}U,^{235}U, ^{239}Pu, and ^{241}Pu nuclei was studied in Ref. [18], where triton and alpha particles were detected along with two fission fragments. The study concluded that the probability of long range alpha (LRA) particle emission increases with an increase in fissility parameters.

Pyatkov *et al*. [19, 20] performed an experiment to study the spontaneous fission of ^{252}Cf nucleus and thermal neutron induced reaction on ^{235}U nucleus within the CCT geometrical channel of the ternary fission. In this experiment, binary coincidences with two detectors placed at a relative angle of 180° were measured, and the third fragment was estimated using the missing mass method. They concluded that there is probability of emission of Sn/Ni or Sn/Ge clusters, and the process may be a simultaneous emission or sequential process. This experiment provided a new view in the field of ternary fission, and numerous approaches have been introduced to explore the CCT process. An analysis of the sequential decay of the ^{235}U($n^{\rm th}$, f) reaction was conducted in Ref. [4] using the DNS model, and the clusters of Ge and Se isotopes along with Ni and Zn isotopes were identified as the probable decaying fragments in the CCT mechanism. After this analysis, sequential ternary decay of ^{252}Cf nucleus was studied by Tashkhodjaev *et al*. [21], where the relative yield of Ni and Sn nucleus was found to be large. Similarly, the sequential emission of the fragments from ^{252}Cf nucleus was studied and the kinetic energy of the fragments calculated in Ref. [22]. The study concluded that the kinetic energy of the middle fragment is the least among the three. The study observed that the kinetic energy depends on the excitation energy of the decaying fragments. Exploring the CCT mechanism using an excitation energy dependent approach would be of further interest. In this paper, a quantum mechanical fragmentation theory (QMFT) based approach is applied to explore the sequential emission of the ^{235}U($n^{\rm th}$, f) reaction. The sequential process is considered to occur in two steps, where the nucleus initially divides into two fragments and one of the fragments further decays via binary fission. The decaying fragments are identified using the fragmentation potential and preformation probability (P_0). The calculations are performed by determining the total excitation energy of the decaying fragments using an iteration process, and the excitation energy is shared using an excitation energy dependent level density parameter.

The primary objectives of this study are (i) to analyze the mass fragmentation of the ^{236}U* nucleus and identify the probable decaying fragments, (ii) calculate the excitation energy of the decay channel and sharing of energy among the decaying fragments, (iii) perform a decay analysis of the heavy fragment at its respective excitation energy, and (iv) obtain the kinetic energy of the identified fragments in exit channel. The remainder of the manuscript is organized as follows. Section II describes the methodology used, and the QMFT based model used to analyze the sequential decay process is briefly discussed. The fragmentation analysis and sharing of the excitation energy is presented in Sec. III. Finally, the summary of the results is provided in Sec. IV.

II. METHODOLOGY

In this study, the sequential decay of the ^{235}U($n^{\rm th}$, f) reaction is investigated within the QMFT framework [23−36]. The decay mechanism is considered in two stages. In the first step, the parent nucleus decays via an asymmetric decay channel A_1+A_2, and in the second step, the heavier fragment A_2 should break into two fragments A_3 and A_4. The pictorial representation of this mechanism is shown in Fig. 1. The partitioning of the nucleus is considered along the fission axes in both of the stages. Here, the heavier fragment of the stage I does not change the momentum direction when it divides into two fragments. The decay of the compound nucleus is analyzed using the excitation energy and an excitation energy dependent level density parameter. The total excitation energy of the fission fragments is given [37, 38] as follows:

$$E^* = E_f^* + Q - V, \tag{1}$$

where E_f^* is the excitation energy of the fissioning parent

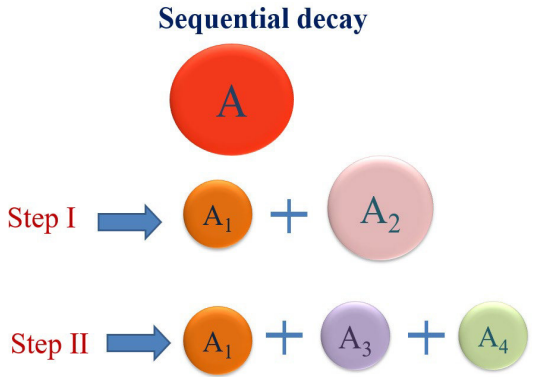

Fig. 1. (color online) Pictorial representation of the sequential decay of the Collinear cluster tripartition (CCT).

nucleus, V is the interaction potential of the decay channel, and Q is the Q-value of the decay channel. The calculations are performed at temperature T, which is related to the total excitation energy E^* as

$$E^* = a_i(E^*)T^2 - T, \tag{2}$$

here, $a_i(E^*)$ denotes the excitation energy dependent level density parameter [37, 39], expressed as

$$a_i(E^*) = a_i(A_i)\left(1 + \frac{1-\exp(E^*/E_D)}{E_i^*}\delta U_i\right), \tag{3}$$

here, $a_i(A_i)$ is obtained from [40]:

$$a_i(A_i) = 0.1337A_i - 0.06571A^{\frac{2}{3}} \tag{4}$$

and E_D=18.5 MeV. After T is calculated, the fragmentation potential is calculated as

$$V_R(\eta,T) = \sum_{i=1}^{2}[V_{LDM}(A_i,Z_i,T)] + \sum_{i=1}^{2}[\delta U_i]\exp(-T^2/T_0^2) + V_C(R,Z_i,\beta_{\lambda i},\theta_i,T) + V_P(R,A_i,\beta_{\lambda i},\theta_i,T). \tag{5}$$

Here, V_{LDM} is the temperature dependent macroscopic liquid drop potential values obtained from Davidson *et al.* [41]. δU denotes the "empirical" microscopic shell correction as given in [42]; additionally, it is made T-dependent to vanish exponentially with T_0=1.5 MeV [43]. For both V_{LDM} and δU, the parts of the binding energy (B.E.) are obtained using the macro-microscopic re-normalization method of Strutinsky [44]. δU is strongly affected by the E^* of the nucleus (see Eq. (5)) and begins fading at sufficiently higher energies [43]. The "optimum" orientations $\theta_i^{\text{opt.}}$ for the hot-compact and cold-elongated configurations are obtained from Table 1 of Ref. [45]. The deformation values are obtained from Ref. [46]. In Eq. (5), V_C and V_P are the Coulomb and proximity potentials, respectively (for a description, see Ref. [29, 47]). The fragmentation potential $V_R(\eta, T)$ is futher employed to calculate the preformation yields $P_0(A_i)$ of the decaying fragments (A_i), which is obtained by solving the Schrödinger equation in η-coordinate at fixed $R = R_a$,

$$\left\{-\frac{\hbar^2}{2\sqrt{B_{\eta\eta}}}\frac{\partial}{\partial\eta}\frac{1}{\sqrt{B_{\eta\eta}}}\frac{\partial}{\partial\eta} + V_R(\eta,T)\right\}\psi^{\nu}(\eta) = E^{\nu}\psi^{\nu}(\eta), \tag{6}$$

where $\nu = 0,1,2,3...$ referring to ground state ($\nu = 0$) and excited state solutions, with the ground state preformation probability P_0 given as

$$P_0 = |\psi(\eta(A_i))|^2\sqrt{B_{\eta\eta}}\frac{2}{A_{CN}}. \tag{7}$$

The higher values of ν also contribute to the excited states, and these contributions enter via excitation of higher vibrational states. For these excited states, the wave function is given by

$$|\psi|^2 = \sum_{\nu=0}^{\infty}|\psi^{\nu}|^2\exp(-E^{\nu}/T). \tag{8}$$

P_0 is the probability of finding certain mass fragments at position R on the decay path and is calculated using collective clusterization to estimate the fission products. $B_{\eta\eta}$ in Eq. (7) represents the smooth hydrodynamical mass parameter [48]. Furthermore, for the binary fission, the total excitation energy E^* should be distributed among the two fission fragments and is proportional to their level density parameters. Based on this, the excitation energy between the decaying fragments is calculated using the level density parameter [37, 38]:

$$E_i^* = \frac{E^*a_i}{a_1 + a_2}, \tag{9}$$

here, E_i^* denotes the excitation energy of one of the de-

Table 1. Calculated Q-value, proton and neutron numbers, and barrier height for the spherical and cold choices of decay fragments.

Decay channel	Q Value/MeV	Barrier height/MeV		(N_1,Z_1)+(N_2,Z_2)
		Spherical	Cold	
^{70}Ni+^{166}Gd	158.64	187.79	176.54	(42,**28**)+(102,64)
^{72}Ni+^{164}Gd	158.41	188.64	177.51	(44,**28**)+(102,64)
^{80}Ge+^{156}Nd	174.33	193.69	186.64	(48,32)+(96,60)
^{82}Ge+^{154}Nd	177.59	199.95	189.26	(**50**,32)+(94,60)

cay fragment, and a_i represents the corresponding level density parameter.

III. CALCULATIONS AND DISCUSSIONS

This section represents the sequential decay analysis of the ^{235}U(n^{th}, f) reaction using the temperature dependent fragmentation approach. The decay mechanism is considered to occur in two stages. In the first stage, one of the three fragments is identified along with a complementary heavy fragment. The total excitation energy of the decay channel is calculated and is divided among the two fragments using the level density parameter. The heavy fragment further divides into two fragments owing to its instability in the second stage. First, Sec. III.A analyzes the fragmentation of the ^{236}U* nucleus using the fragmentation potential, and the preformation probability and most probable decaying fragments are identified. The barrier characteristics of the identified decay channels are compared for light and heavy fragments as the first fragments of the sequential emission. Subsequently, in Sec. III.B, the total excitation energy of the decay channel is calculated using an iteration process, and the sharing of the excitation energy among the fragments is estimated using the excitation energy dependent level density parameter. In Sec. III.C, the decay of the heavy fragment in stage I is presented, and fragments of the sequential fragmentation are identified. The kinetic energy of each fragment is calculated, and related dynamics are explored. Sec. IV summarizes the observed results.

A. Decay analysis of ^{236}U* nucleus and identification of the probable fragments

In this section, stage I of the decay of the^{236}U* nucleus is analyzed using the fragmentation potential and preformation probability. First, the fragmentation potential is calculated for the ^{236}U* nucleus at E^* = 6.55 MeV (excitation energy of the nucleus due to thermal energy induced by neutrons) for the spherical and deformed choices of the decaying fragments. The calculated fragmentation potential is plotted as a function of fragment mass A_1 in Fig. 2 for the (a) spherical and (b) deformed (cold) choices of the decaying fragments. Note that the decay fragments with the minimum fragmentation potential value (or present at the dips of the fragmentation structure) represent the most probable decay channel.

It is evident from the figure that the asymmetric fission distribution is obtained for the spherical and deformed choices of the decaying fragments. The experimental observations of [49] support the asymmetric mass distribution for the ^{235}U(n^{th}, f) reaction; hence, our results agree with the experiment. Furthermore, in the experimental observation of the CCT [18, 19] of the ^{235}U(n^{th}, f) reaction, ^{68,70,72}Ni and ^{80,82}Ge fragments were detected along with complementary ^{128,130,132}Sn fragments, and the third fragment was detected using the missing mass approach. As our analysis is a sequential process, among the three decay fragments, Fragment A_1 obtained in step I is identified and compared with an experimentally observed fragment. The other two fragments A_3 and A_4 are identified in Sec. III.C. Fragment A_1 of the experimentally observed CCT decay channel lies in 68−82 mass region. Hence, to identify A_1, we have plotted the fragmentation potential for A_1= 60−90 in inset of Fig. 2 for the (a) spherical and (b) β_2-deformed choices of the decaying fragments. Here, the dips of the fragmentation potential represent the probable decaying fragments. We observe from the fragmentation structure that ^{70}Ni, ^{72}Ni,

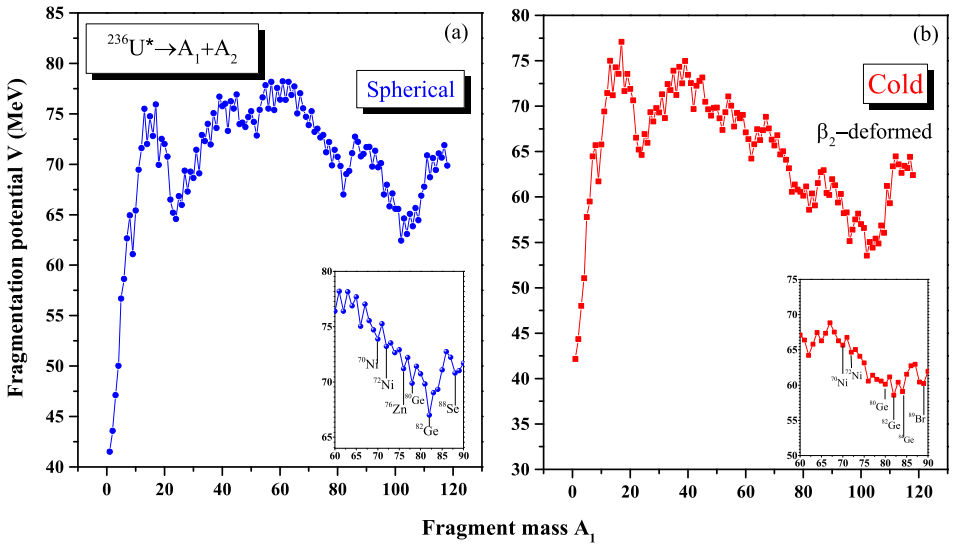

Fig. 2. (color online) Fragmentation potential V plotted as a function of fragment mass A_1 for the (a) spherical and (b) deformed choices of the decaying fragments. The inset of the figures represents the fragmentation potential for A_1=60−90.

^{76}Zn, ^{80}Ge, ^{82}Ge, and ^{88}Se represent the most probable A_1 fragments for the spherical choice of the decaying fragments. For the β_2-deformed choice of the fragments, the identified fragments A_1 are ^{70}Ni, ^{72}Ni, ^{76}Zn, ^{80}Ge, ^{82}Ge, ^{84}Ge, and ^{89}Br. The identified fragments ^{70}Ni, ^{72}Ni, ^{80}Ge, and ^{82}Ge were also detected in the experimental results. Hence, the first step of our analysis agrees with the experimental observation [19]. After the fragmentation potential, the other factor used to identify fragments is the preformation probability of the decaying fragments. The preformation probability is calculated by solving Schrödinger's equation in the η-coordinate and plotted as a function of fragment mass A_i (i=1,2) for the (a) spherical and (b) deformed choices of the decaying fragments. This is shown in Fig. 3. Note that the preformation distribution also supports asymmetric fission distribution for both spherical and β_2-deformed choices of the decaying fragments as we observed using the fragmentation structure. Here, the peaks in the preformation probability represent the most probable fragments. The insets in Fig. 3 (a) and (b) represent the preformation probability values for A_1=65−85. The identified fragments are ^{70}Ni, ^{72}Ni, ^{80}Ge, and ^{82}Ge for both spherical and deformed choices of the fragments. Hence, ^{70}Ni, ^{72}Ni, ^{80}Ge, and ^{82}Ge are considered the most probable A_1 fragments of stage I. These identified decay fragments and their complementary fragments lie near the proton and neutron shell closure.

It is important to mention here that, in the experimental observation, heavy Sn fragments were observed, and these fragments are evident in the calculated fragmentation structure and preformation probability distribution for both choices of the decaying fragments. These Sn fragments may be emitted along with complementary fragments in the first stage of the sequential analysis. It will be of interest to observe which of these two choices dominate in stage I. For this analysis, the scattering potential of the light A_1 and heavy (Sn) A_1 fragments is calculated and plotted as a function of the R-coordinate, as shown in Fig. 4 for the spherical choice of the decaying fragments. The figure shows that the barrier height of the decay channel increases with an increase in the mass number of the light A_1 fragment (see Fig. 4 (a)) and almost equal for the heavy A_1 fragment (see Fig. 4 (b)). The light A_1 fragment combinations of Fig. 4 (a) have a lower barrier height than the heavy A_1 fragment combinations (Fig. 4 (b)). The barrier characteristics are also studied using the deformed choice of the decaying fragments and are shown in Fig. 5. Note that the barrier height is relatively lower for the deformed choice than for the spherical choice of the decaying fragments. The difference in the barrier height is basically due to the larger Coulomb repulsion and the change in the nuclear proximity potential. The light A_1 fragment has a lower barrier height than the heavy one for both spherical and deformed choices of the decaying fragments. Hence, we may conclude that the light A_1 fragments are more probable than the heavy A_1 fragment in stage I. After this analysis, the excitation energy of the decaying fragments is calculated and the results are discussed in the next section.

B. Sharing of the excitation energy using level density parameter

In the previous section, the decay channel is identified using the fragmentation potential and preformation probability. Furthermore, the barrier characteristics of the

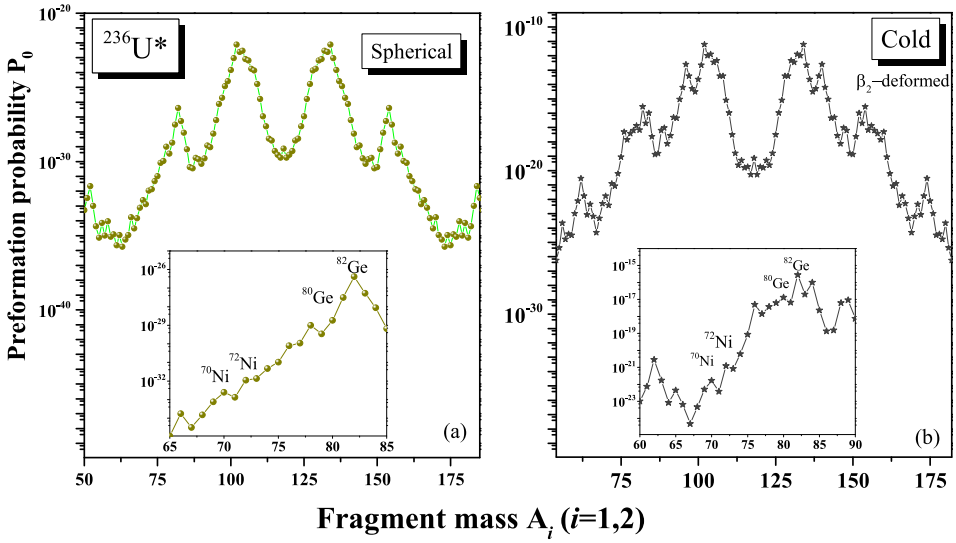

Fig. 3. (color online) Calculated preformation probability P_0 plotted as a function of fragment mass A_i, (i=1,2) for the (a) spherical and (b) deformed choices of the decaying fragments. The insets represent the preformation probability for (a) A_1= 65−85 and (b) A_1= 60−90.

decay channel are studied, and ^{70}Ni, ^{72}Ni, ^{80}Ge, and ^{82}Ge are considered the most probable A_1 fragments of stage I. In this section, the total excitation energy of the decay channel is calculated using the scattering potential at the touching configuration of the decaying fragments.

The QMFT uses the terms of the mass asymmetry coordinate (η) and relative separation coordinate (R). After the preformation analysis using mass asymmetry coordinate (η), the subsequent decay dynamics are examined using the scattering potential (V), which is calculated in terms of the R-coordinate. The scattering potential is calculated for the decay channel ^{70}Ni+^{166}Gd and is shown in Fig. 6 at $T = 0$ MeV. Note that the total excitation energy of the decay channel can be calculated by subtracting the interaction potential value from the sum of the Q value and E^*(see Eq. (1)). Furthermore, the barrier height for the spherical and the cold choice of the identified decay channels are calculated and listed in Table 1. The table also presents the calculated Q value and shell effects associated with the decay channel. Note from the table that the Q-value of the decay channel increases with an increase in the size of the smaller fragment. Furthermore, the barrier height of the decay channel increases with an increase in the size of the A_1 fragment. All the identified decay fragments lie in the neighbourhood of proton and neutron shell closure.

The total excitation energy is calculated using an iteration process using Eq. (1), where the scattering potential is initially calculated at $T = 0$ MeV, and the corresponding $E_{\rm I}^*$ is obtained. Furthermore, using this $E_{\rm I}^*$, we obtain the total excitation energy ($E_{\rm II}^*$) of the decay channel. This approach is used in Refs. [37, 38], which consider that the damping of the shell effects is small at the obtained excitation energies of the fission fragments. First, the excitation energy is obtained using $T = 0$ MeV. For the four cases, ^{70}Ni+^{166}Gd, ^{70}Ni+^{166}Gd, ^{80}Ge+^{156}Nd, and ^{82}Ge+^{154}Nd, the excitation energies are calculated and shown in Fig. 7. The figure indicates that for the spherical choice of the decaying fragments, the excitation energy increases up to ^{80}Ge and decreases for ^{82}Ge. After this strange observation of the excitation energy of the decay channel ^{82}Ge+^{154}Nd, the deformation effects are included [46] (β_{21}= 0.053, β_{22}= 0.270). As a next step, the excitation energy is calculated using the deformed choice of the decaying fragments. For the deformed choice of the decaying fragments, the excitation energy increases with an increase in fragment mass. Hence, the deformation effects play an important role in the estimation of the excitation energy of the decaying fragments.

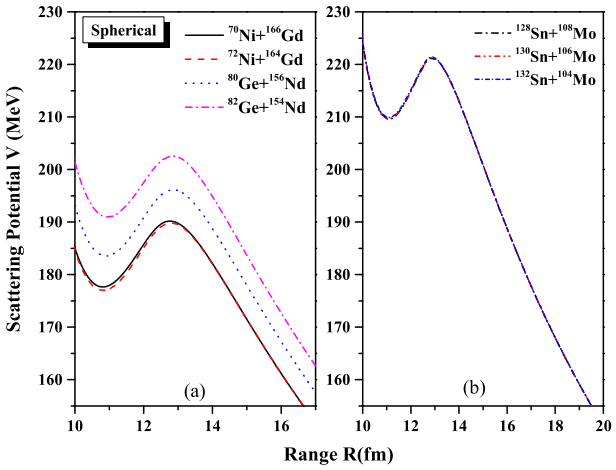

Fig. 4. (color online) Calculated scattering potential as a function of the R-coordinate for the (a) light and (b) heavy A_1 fragments using a spherical choice of the decaying fragments.

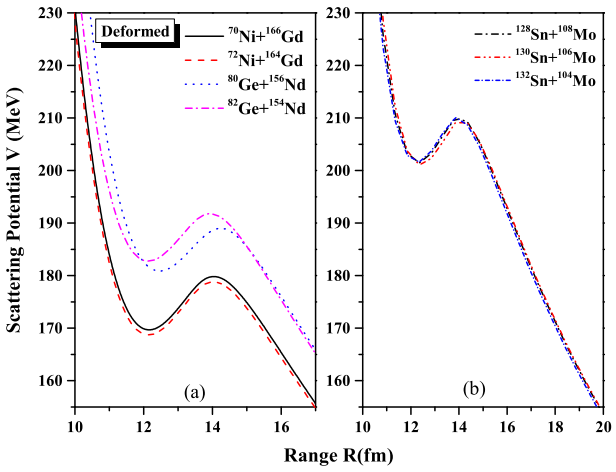

Fig. 5. (color online) Calculated scattering potential as a function of the R-coordinate for the (a) light and (b) heavy A_1 fragment using a deformed choice of the decaying fragments.

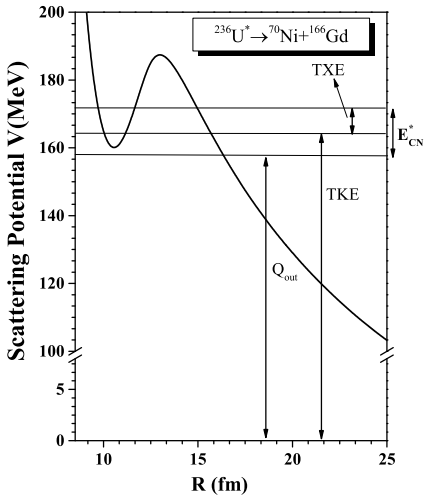

Fig. 6. Calculated scattering potential of the decay channel as a function of the R-coordinate. The total excitation energy of the decay channel can be calculated using $Q_{\rm out}$ and E^* and can be easily observed in the figure.

After the calculation of the excitation energy (E_I^*) at $T = 0$ MeV, the level density parameter at these excitation energy is calculated using Eq. (3). This level density parameter is used to calculate the value of E_{II}^* using Eq. (1). For this process, temperature dependent binding energies (TDBEs) are calculated at their respective T values. Using these TDBEs, we calculate Q_{out} and estimate the interaction potential at respective T values. The calculated value of the E_f^*+Q and the scattering potential V is plotted as a function of fragment mass A_1 for the spherical choice of the decaying fragments and shown in Fig. 8. We observe that the E_f^*+Q value is higher than V value for ^{70}Ni and ^{72}Ni. Furthermore, the value is lower for the ^{80}Ge and ^{82}Ge fragments, which correspond to a negative E^* value. Similar results can be observed in Fig. 9, which presents the values obtained using the deformed choice of the decaying fragments. Hence, the fragment combinations ^{70}Ni + ^{166}Gd and ^{72}Ni + ^{164}Gd are more probable decay channels than ^{80}Ge + ^{156}Nd and ^{82}Ge + ^{154}Nd. Similar analysis is made in Ref. [50], where the emission probability of the heavy fragments increased with a higher value of E_f^*. Hence, we proceed with ^{70}Ni and ^{72}Ni along with their complementary fragments. The obtained values of E_{II}^* for the ^{70}Ni and ^{72}Ni decay channels are 4.91 and 5.93, respectively, for the spherical choice and 4.52 and 11.40, respectively, for the deformed choice of the decaying channel. Thereafter, the level density parameter for both of the fragments is calculated at this excitation energy, and the sharing of the excitation is performed using the relation Eq. (9). The shared excitation energy of each fragment of the decay channel for the spherical and deformed choice is shown in Table 2. The heavy fragment has a higher value of the excitation energy than the lighter fragment. The decay of the heavy fragment A_2 at this excitation energy is analyzed in the next section.

C. Decay analysis of the heavy fragment A_2 at the respective excitation energy

In the previous section, ^{70}Ni+^{166}Gd and ^{72}Ni+^{164}Gd channels are identified as the probable decay channels of the ^{235}U(n^{th}, f) reaction. The excitation energy of the decay channels is calculated. We also observe that the heavy fragment (A_2) of the decay channel has more excitation energy than the light fragment (A_1). Hence, the probability of splitting of a heavy fragment is higher than that of light fragments. It is relevant to note that, the decay analysis of Gd isotopes was made in Ref. [51], and concluded that these nuclei may lead to heavy Sn isotopes as daughter fragment. The fissile nature of various nuclei was also studied in Ref. [52], which showed that the nuclei whose fissility parameter lie between 30.5 and 43.3 are more favourable as the three fragment emission. The fissility parameter for ^{236}U nucleus is 35.86; hence,

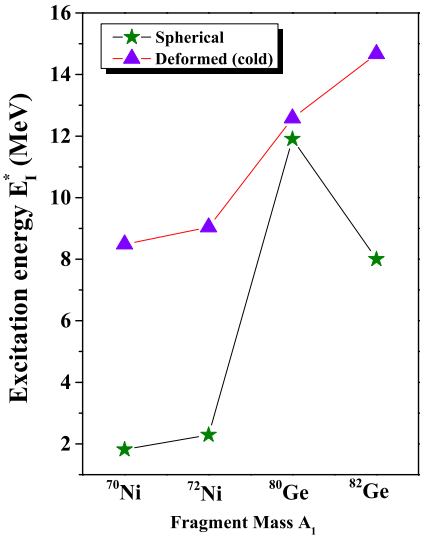

Fig. 7. (color online) Calculated excitation energy (MeV) for the identified decaying fragment.

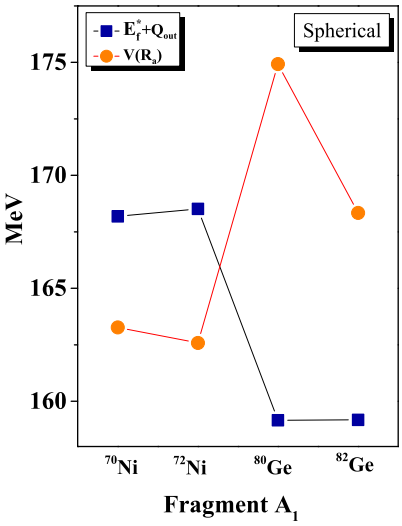

Fig. 8. (color online) Graphical representation of Ef^*+Q_{out} and the interaction potential value at touching state for the spherical choice of decaying fragments.

three fragment emission is probable for this nucleus. The abovementioned points demonstrate that the three fragment emission is applicable for the ^{236}U nucleus. Hence, the Gd isotopes can further exhibit binary division. First, the fragmentation potential is calculated, as shown in Fig. 10, for the ^{164}Gd and ^{166}Gd nuclei for the (a,c) spherical and (b,d) deformed choices of the decaying fragments for A_3=25−45. The most probable decaying fragment combination A_3+A_4 can be obtained with reference to the dips in the fragmentation structure. The obtained combination of the decaying fragments is marked in the figure and is shown in Table 3. The table shows that the identified fragment pairs remain unchanged independent of the deformation effect. The most probable decaying fragment

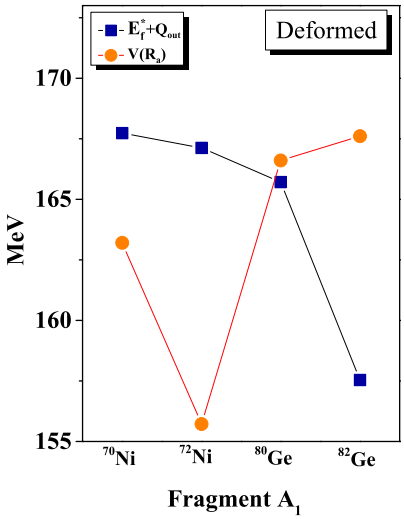

Fig. 9. (color online) Graphical representation of $E_f{}^*+Q_{\rm out}$ and the interaction potential value at touching state for the deformed choice of decaying fragments.

Table 2. Shared energy values E_1 and E_2 of the excitation energy $E_{\rm II}{}^*$ in MeV for the fragments A_1 and A_2 using excitation energy based level density parameter.

Decay channel	Spherical		Deformed	
	E_1^*	E_2^*	E_1^*	E_2^*
^{70}Ni+^{166}Gd	3.817	1.095	3.902	1.115
^{72}Ni+^{164}Gd	4.891	1.995	8.765	2.635

combination contains Mg, Te, Si. and Sn isotopes.The obtained decaying fragments lie near the neutron and proton shell closure. In the experimental attempt of CCT, isotopes of Ni, Si, and Sn are obtained, and the third fragment is identified using the missing mass method. This analysis shows that Si isotopes may appear as the middle fragments. In addition, the Mg and S isotopes appear along with Te or Cd isotopes in the second step of the CCT mechanism. An experimental verification of these fragments would be of further interest.

After identifying the A_3 and A_4 fragments, we analyze the recognition of the middle and side fragment of the CCT mechanism. This is accomplished by calculating the total kinetic energy (TKE) of the decaying fragments. After the decaying fragments are identified, the kinetic energy of these channels is calculated using the TKE relation from Ref. [53]:

$$TKE = \frac{0.2904(Z_1+Z_2)^2}{A_1^{1/3}+A_2^{1/3}-(A_1+A_2)^{1/3}}\frac{A_1A_2}{(A_1+A_2)^2}. \quad (10)$$

The kinetic energy is shared using the reduced mass concept, and the obtained values of the kinetic energy of each fragment are shown in Fig. 11. Note that the kinetic energy is higher for the Sn fragments and lower for Ni

Table 3. Most probable decay channel obtained in stage II for ^{164}Gd and ^{166}Gd nuclei for the spherical and deformed choices of the decaying fragments.

S.	^{164}Gd		^{166}Gd	
no.	Spherical	Deformed	Spherical	Deformed
1.	^{30}Mg+^{134}Te	^{30}Mg+^{134}Te	–	–
2.	^{32}Mg+^{132}Te	^{32}Mg+^{132}Te	^{32}Mg+^{134}Te	^{32}Mg+^{134}Te
3.	^{34}Si+^{130}Sn	^{34}Si+^{130}Sn	^{34}Si+^{132}Sn	^{34}Si+^{132}Sn
4.	^{36}Si+^{128}Sn	^{36}Si+^{128}Sn	^{36}Si+^{130}Sn	^{36}Si+^{130}Sn
5.	^{38}Si+^{126}Sn	^{38}Si+^{126}Sn	^{38}Si+^{128}Sn	^{38}Si+^{128}Sn
6.	^{40}S+^{124}Cd	^{40}S+^{124}Cd	–	–

isotopes. In contrast, the Si isotopes have the least value compared with the other two fragments of the decay channel. Hence, the Si fragment is the middle fragment of the decay channel. Similar results were obtained for ^{252}Cf isotopes in Ref. [22], where the kinetic energy of the middle fragment was significantly lower than those of the other two fragments. Hence, the kinetic energy of the middle fragment remains low in spontaneous and induced fission processes.

IV. SUMMARY

The decay of the ^{235}U($n^{\rm th}$, f) reaction is analyzed using a QMFT based approach. CCT is studied as a sequential process, where the nucleus division occurs in two stages. In the first stage, the nucleus divides into asymmetric fragments, and the heavier fragment further divides into two fragments. Stage I is analyzed using the fragmentation potential and preformation probability for the spherical and deformed choices of the decaying fragments. The most probable A_1 fragments identified are ^{70}Ni, ^{72}Ni, ^{80}Ge, and ^{82}Ge nuclei. In addition, the fragmentation structure suggests heavy Sn isotopes as probable decaying fragments. We compare the barrier characteristics of the light fragments (^{70}Ni, ^{72}Ni, ^{80}Ge, and ^{82}Ge) and heavy Sn isotopes and observe that lighter fragments have a higher emission probability.

The excitation energy of the identified decay channels is calculated using an iteration process. Initially, the excitation energy $E_{\rm I}^*$ is calculated, which increases with an increase in the fragment mass A_1 of the decay channel for the deformed choice of the decaying fragments. This energy is further used to calculate the total excitation energy $E_{\rm II}^*$ of the decaying fragments using the temperature dependent binding energies (TDBEs) and temperature dependent interaction potential. In this process, ^{70}Ni+^{166}Gd and ^{72}Ni+^{164}Gd are observed to be the most probable decay channels. The obtained $E_{\rm II}^*$ is shared among the decaying fragments using an excitation energy dependent level density parameter. The fragmentation of the ob-

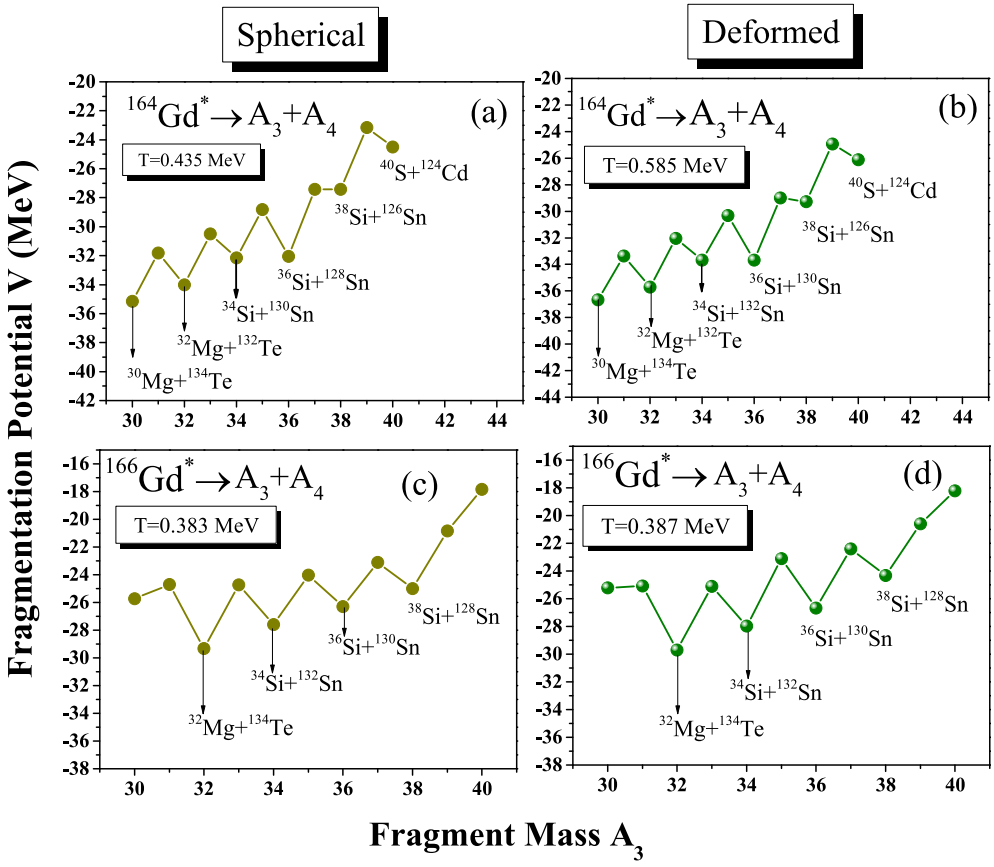

Fig. 10. (color online) Fragmentation potential V for $^{164,166}Gd^{*}$ calculated as a function of fragment mass $A_3 = 25-45$ for the spherical and deformed choices of the decaying fragments.

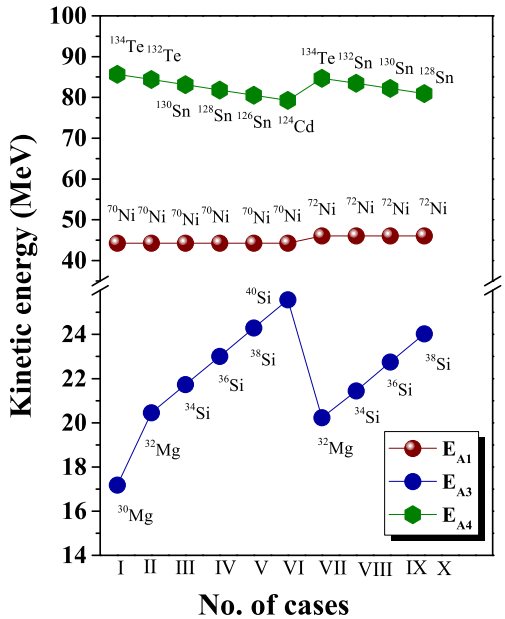

Fig. 11. (color online) Calculated kinetic energies of the three fragments for the cases obtained in stage II of the sequential decay mechanism.

tained heavier fragments (^{166}Gd and ^{164}Gd) is analyzed at corresponding shared excitation energies. The identified A_3 and A_4 fragments are ^{30,32}Mg, $^{34-40}$Si, $^{126-132}$Sn, and ^{132,134}Te, respectively. The identified decay channel containing Ni, Si, and Sn isotopes agree with experimental observations. The fragmentation structure also suggest few additional tri-partition combinations containing Ni, Mg, Sn, and Cd isotopes, for which experimental verification would be of further interest. The total kinetic energy of the decay fragments is calculated for both stages, and the energy sharing is estimated using the reduced mass approach. The middle fragment of the sequential CCT mechanism is identified using the kinetic energy of the fragments. The fragmentation of the CCT mechanism as a simultaneous process (where three fragment emissions occur simultaneously) and comparison with the sequential process would be of further interest.

ACKNOWLEDGEMENT

The financial support from the Department of Science and Technology (DST), New Delhi, India, in the form of a research project (File no. CRG/2021/001144) is gratefully acknowledged.

References

[1] O. Hahn and F. Strassmann, Naturwissenschaften **89**, 27 (1939)
[2] A. V. Ramayya, J. K. Hwang, J. H. Hamilton *et al*., Phys. Rev. Lett. **81**, 947 (1998)
[3] Yu. N. Kopatch, M. Mutterer, D. Schwalm *et al*., Phys. Rev. C **65**, 044614 (2002)
[4] R. B. Tashkhodjaev, A. K. Nasirov, and W. Scheid, Eur. Phys. J. A **47**, 136 (2011)
[5] D. N. Poenaru, W. Greiner and R. A. Gherghescu, At. Nucl. Data Table **68**, 91 (1998)
[6] R. A. Gherghescu, W. Greiner, and D. N. Poenaru, Int. J. Mod. Phys. E **17**, 2221 (2008)
[7] D. N. Poenaru, W. Greiner, and R. A. Gherghescu, Nucl. Phys. A **747**, 182 (2005)
[8] V. I. Zagrebaev, A. V. Karpov, and W. Greiner, Phys. Rev. C **81**, 044608 (2010)
[9] A. V. Karpov, Phys. Rev. C **94**, 064615 (2016)
[10] A. K. Nasirov, R. B. Tashkhodjaev, and W. von Oertzen, Eur. Phys. J. A **52**, 135 (2016)
[11] N. Sharma, A Kaur, and M. K. Sharma, Phys. Rev. C **105**, 044602 (2022)
[12] D. N. Poenaru *et al*., Phys. Rev. C **59**, 6 (1999)
[13] K. Manimaran and M. Balasubramaniam, Phys. Rev. C **83**, 034609 (2011)
[14] H. Diehel and W. Greiner, Nucl. Phys. A **229**, 29 (1974)
[15] G. Royer and J. Mignen, J. Phys. G: Nucl. Part. Phys. **18**, 1781 (1992)
[16] H. Diehel and W. Greiner, Phys. Lett. B **45**, 35 (1973)
[17] H. W. Schmitt *et al*., Phys. Rev. Lett **9**, 10 (1962)
[18] C. Wagemans *et al*., Phys. Rev. C **33**, 3 (1986)
[19] Yu.V. Pyatkov *et al*., Eur. Phys. J. A. **45**, 9 (2010)
[20] Yu.V. Pyatkov *et al*., Physics of atomic nuclei **73**, 1309 (2010)
[21] R. B. Tashkhodjaev *et al*., Phys. Rev. C **91**, 054612 (2015)
[22] K. R. Vijayraghvan *et al*., Eur. Phys. J. A. **48**, 27 (2012)
[23] G. Sawhney, M. K. Sharma, and R. K. Gupta, Phys. Rev. C **83**, 064610 (2011)
[24] K. Sharma, G. Sawhney, M. K. Sharma *et al*., Nucl. Phys. A **1**, 972 (2018)
[25] A. Kaur and M. K. Sharma, Phys. Rev. C **99**, 044611 (2019)
[26] A. Kaur and M. K. Sharma, Eur. Phys. J. A **55**, 89 (2019)
[27] G. Kaur, K. Sandhu, A. Kaur *et al*., Phys. Rev. C **97**, 054602 (2018)
[28] A. Kaur, G. Kaur, S. K. Patra *et al*., Nucl. Phys. A **990**, 94 (2019)
[29] B. B. Singh, M. K. Sharma, and R. K. Gupta, Phys. Rev. C **77**, 054613 (2008)
[30] M. K. Sharma *et al*., Phys. Rev. C **93**, 014322 (2016)
[31] M. Kaur and M. K. Sharma, Phys. Rev. C **85**, 054605 (2012)
[32] M. Kaur and M. K. Sharma, Eur. Phys. J. A. **50**, 61 (2014)
[33] K. Sharma *et al*., Nucl. Phys. A. **972**, 1 (2018)
[34] H. J. Fink, J. Maruhn, W. Scheid *et al*., Z. Phys. **268**, 321 (1974)
[35] J. Maruhn and W. Greiner, Phys. Rev. Lett. **32**, 548 (1974)
[36] R. K. Gupta, W. Scheid, and W. Greiner, Phys. Rev. Lett. **35**, 353 (1975)
[37] A. V. Andreev, G. G. Adamian, N. V. Antonenko *et al*., Eur. Phys. J. A **30**, 579 (2006)
[38] A. V. Andreev, G. G. Adamian, N. V. Antonenko *et al*., Eur. Phys. J. A **22**, 51 (2004)
[39] S. Hilaire, Phys. Lett. B **583**, 264 (2004)
[40] T. Rauscher, F.-K. Thielemann, and K.-L. Kratz, Phys. Rev. C **56**, 1613 (1997)
[41] N. J. Davidson, S. S. Hsiao, J. Markram *et al*., Nucl. Phys. A **570**, 61c (1994)
[42] W. Myers and W. J. Swiatecki, Nucl. Phys. **81**, 1 (1966)
[43] A. S. Jensen and J. Damgaard, Nucl. Phys. A **203**, 578 (1973)
[44] V. M. Strutinsky, Nucl. Phys. A **95**, 420 (1967)
[45] R. K. Gupta, M. Balasubramaniam, R. Kumar *et al*., J. Phys. G: Nucl. Part. Phys. **31**, 631 (2005)
[46] P. Möller, J. R. Nix, W. D. Myers *et al*., At. Data Nucl. Data Tables **59**, 185 (1995)
[47] R. Kumar and M. K. Sharma, Phys. Rev. C **85**, 054612 (2012)
[48] H. Kröger and W. Scheid, J. Phys. G: Nucl. Part. Phys. **6**, L85 (1980)
[49] A. C. Wahl, At. Data Nucl. Data Tables **39**, 1 (1988)
[50] C. Karthikraj and Z. Ren, Phys. Rev. C **101**, 014603 (2020)
[51] K. Sharma *et al*., Eur. Phys. J. A. **55**, 30 (2019)
[52] W.J. Swiatecki, Geneva **15**, 651 (1958)
[53] C. M. Herbach *et al*., Nucl. Phys. A **712**, 207 (2002)